Two-Crystal Neutron Interferometry

A. Zeilinger[†], C. G. Shull, M. A. Horne[††], and G. L. Squires[†††]
Massachusetts Institute of Technology*
Cambridge, Mass., 02139, U.S.A.

Abstract

Observations are reported on the performance of a neutron interferometer using two successive Laue reflections from separated, thick crystal plates. The interferometer makes explicit use of coherence characteristics within the Borrmann fan associated with dynamical diffraction theory. The spatial distribution of the intensity released from the interferometer and the interference effects in the two beams leaving the central focal point have been studied and compared with theoretical prediction.

*The research program reported here has been supported by grants from the National Science Foundation and the Department of Energy.

[†]Permanent address: Atominstitut der Österreichischen Universitäten, Wien, Österreich.

[††] " " : Stonehill College, North Easton, Mass.

[†††] " " : Cavendish Laboratory, Cambridge, England

I. Introduction

Perfect crystal neutron interferometry was first demonstrated by Rauch, Treimer and Bonse (1974) with a three-crystal system in Laue-geometry. The wide separation between the coherent beams in this type of interferometer has made possible a number of significant experiments, most notably those dealing with the neutron-gravitational potential interaction and the Fermion spin-rotation. Interpretation of these experiments was not critically dependent upon a detailed description of the diffraction processes occurring in the three crystal plates that form this type of interferometer. Although several authors, Rauch and Suda (1974), Bauspiess *et. al.* (1976) and Petraschek and Folk (1976) have developed theories of this interferometer type, no detailed experimental confirmation of the theory has been attempted. On the other hand, the theoretical predictions of Kato (1960, 1961) of wave propagation in a single plate of perfect crystal in Laue geometry have been confirmed in considerable detail for the neutron case by Shull (1968, 1973), Shull and Oberteuffer (1972).

Preliminary to performing the presently reported investigations of the diffraction processes occurring in the simpler case of a two-crystal interferometer, it was observed that there was interference action within one beam of a normal three-crystal interferometer as illustrated in Fig. 1. Here the forward diffracted beam was stopped behind the first crystal plate by a Cd absorber thus leaving only one beam path open. The interference action within this beam was studied by transverse scanning through this beam of a multiple step phase plate of Al and observing the intensity released from the interferometer in the two characteristic directions. The step heights in this phase plate were consecutively $\frac{1}{2}D$, D, $\frac{3}{2}D$,..., where D is the λ-thickness, and the

plateau width was wider than the beam width of 1.25 mm. In this interferometer, the individual crystal plate thickness was 2.464 mm with Si(220) reflection being used in symmetrical arrangement with a neutron wavelength of 1.46 Å.

It is seen from the intensity patterns of Fig. 1 that complementary effects are being sensed in the two emergent beams whenever step edges corresponding to odd-π phase difference are passed through the beam, with however no effect at positions corresponding to even-π phase difference. Moreover the fact that the intensity perturbations in the two emergent beams are not quantitatively complementary suggests the presence of additional interference action in the other beam leaving the second crystal plate (not shown in the figure). Additional experiments sensing the intensity in this beam indeed confirmed this.

In view of this demonstration of internal interference action within one beam, it was decided to prepare a two-crystal interferometer with thicker crystal plates and larger separation distance so that the effects could be studied more carefully. For this purpose, an interferometer was cut in the usual monolithic fashion from a Si crystal ingot which had been grown parallel to the [111] axis (see Fig. 2). In order to obtain a long path length between crystal plates, the (400) diffracting planes in symmetric Laue-geometry were selected for use with 1.46 Å neutrons. The plate thickness was 9.210 mm and the separation distance was 37.6 mm. The surfaces were lightly etched to a depth of 6 μm with monitoring by neutron surface reflectivity to ensure the removal of the mosaic layer. With this geometry the full width of the Borrmann fan at the exit face of the first crystal was 11.75 mm and the transverse width of the beam travelling to the second crystal was 9.90 mm. For the (400)

reflection and the above neutron wavelength of 1.46 Å (obtained from a pyrolytic graphite monochromator), the Pendellösung period is calculated to be 92.9 μm. All of the present experiments have been performed with an entrance beam of width 1.07 mm as defined by tapered gadolinium edges.

As is common experience with neutron interferometer systems, it was necessary to provide vibration isolation and this was accomplished by supporting the interferometer on a 25 kg lead pad which was floating on an air-filled rubber tube. Experience with the system showed it to be very sensitive to temperature gradients and it was necessary to enclose the system in a thermal shield box with temperature controlled surroundings. The present experimental observations have concentrated on the distribution of intensity released from the interferometer and on some features of its performance as an interferometer.

II. Intensity Distribution from Interferometer

With entrance position at the first surface being defined by an entrance slit opening, the intensity released from the interferometer has been studied by scanning a slit opening across the exit face of the second crystal with intensity measurement being made simultaneously in both the BF and BB directions. It is to be expected that diffraction focussing will produce a localized intensity peak at the center of the double Borrmann fan at the exit face. This has been predicted for X-rays by the theoretical treatment of Indenbom, Slobodetskii and Truni (1974) with a Green's function approach and verified experimentally by Suvorov and Polovinkina (1974). The effect can also be understood with a ray theory approach. Incoming plane waves slightly off the exact Bragg direction generate in the first crystal two wave fields which travel in different directions $\pm\Omega$ relative to the lattice planes and leave the first crystal at positions $\pm\Gamma$ defined as

$$\Gamma = \frac{\tan \Omega}{\tan \theta_B}$$

These rays propagate parallel to each other to the second crystal where at the entrance face each again generates two wave fields again travelling in $\pm\Omega$ directions. Thus those rays which travelled as different wave fields in the two crystals meet at a focal point on the exit face of the second crystal providing the two crystal plates are of the same thickness. This is true over a range of incident directions and is illustrated in Fig. 3. In the region surrounding the focal point and within the double Borrmann fan, one expects a distributed intensity.

It is evident that divergence effects associated with different wavelength components will cause focussing at slightly different positions on the exit face of the second crystal. In the approach of Indenbom *et. al.* (1974) the intrinsic width of the focal point for purely monochromatic radiation and a δ-function entrance slit is calculated to be 12 μm for our conditions and this is much smaller than the present experimental resolution.

Fig. 4 shows the measured intensity distributions for the two exiting beams in the present interferometer as a function of exit slit position. Strong central peaks (in ratio about 2 to 1) are seen in both beams whose widths are accounted for by the scanning resolution which is much larger than the intrinsic width. A weak, symmetrically distributed intensity out to the edges is seen in the BB beam and a stronger asymmetric distribution is characteristic of the BF beam. The enhanced distributed intensity in the left side of the BF beam (the same orientation sense as in Fig. 2) is characteristic of both the Green's function approach and the plane wave-ray approach. Likewise the symmetric distributed intensity in the BB beam collapsing

to zero intensity at the edges is predicted by both theories. In the plane wave-ray approach, it is necessary to assume incoherence among different incident directions but of course with coherence between the two wave fields in order to obtain agreement with the observed intensity profiles.

III. Interferometer Action

In demonstration of the interference action of this two crystal interferometer, the intensity of the central peak in the two beams has been studied by translating a single-step, phase-plate across the beam between the two crystals. This plate was aluminum with a step height corresponding to a phase difference 3π. The intensity as a function of step position is shown in Fig. 5 with the exit slit held fixed at the central position. The oscillatory intensity patterns, which are complementary in the two beams, demonstrate the presence of interference action.

The character of this oscillation pattern, which was rather unexpected, can be explained phenomenologically by assuming the existence of an intrinsic phase gradient in the interferometer across the Borrmann fan. If this gradient is taken as being constant with the phase changing linearly with Γ and of magnitude ϕ_o in phase difference between Borrmann fan edges, the intensity distribution in the BB central peak beam is expected to be

$$I_{BB}(\Gamma_o) = C \left\{ \int_o^{\Gamma_o} (1-\Gamma^2)^{-1/2} \left[1 + \cos(\phi_o \Gamma)\right] d\Gamma \right.$$

$$\left. + \int_{\Gamma_o}^{1} (1-\Gamma^2)^{-1/2} \left[1 + \cos(\phi_o \Gamma + \pi)\right] d\Gamma \right\}$$

where Γ_o defines the position of the step edge and C is a constant. In this formulation it is assumed that there exists a uniform intensity distribution for all incident directions. Fig. 6 shows the theoretical predictions of the BB intensity for various values of the intrinsic phase difference ϕ_o. A similar expression for the BF beam shows that the two beams are complementary to each other. By comparing the measured intensity variation of Fig. 5 with these calculated curves it can be established that the intrinsic phase difference $\phi_o = 3.7\pi$ was characteristic of the present interferometer. It is seen that the position of the minimum away from the center is a very useful criterion of this phase difference.

A further test on the reality of this intrinsic phase gradient was obtained by compensating for it through insertion of an aluminum wedge in the beam between the two crystals. The wedge had an apex angle of 1.63^o and the effective wedge angle could be varied by tipping around a horizontal axis. With optimum wedge orientation (which agreed with that expected for $\phi_o = 3.7\pi$) the intensity distribution as a function of step edge position is shown in Fig. 7. This clearly exhibits the required shape from Fig. 6 for a phase compensated interferometer. It should be mentioned that, although this intrinsic phase gradient arises from the interferometer fabrication or means of support, it is also very sensitive to temperature gradients of the order of millidegrees/cm.

The approach used to interpret both the intensity distribution from the exit face and the interference profiles with phase step scanning has been plane-wave ray theory assuming no coherence between rays approaching the interferometer from different directions. Future experimentation with smaller entrance slits is expected to elucidate the effects due to coherence between waves of different incident directions.

We wish to acknowledge our indebtedness to J. Callerame who was instrumental in preparing the three crystal interferometer referred to above and to R. Deslattes and A. Henins for assistance in its fabrication.

References

Bauspiess, W., Bonse, U. and Graeff, W. (1976). J. Appl. Cryst. 9, 68.

Indenbom, V.L., Slobodetskii, I., and Truni, K.G. (1974). Sov. Phys. JETP 39, 542.

Kato, N. (1960). Acta Cryst. 13, 349.

Kato, N. (1961). Acta Cryst. 14, 526 and 627.

Petraschek, D. and Folk, R. (1976). phys. stat. sol. (a) 36, 147.

Rauch, H. and Suda, M. (1974). phys. stat. sol. (a) 25, 495.

Rauch, H., Treimer, W. and Bonse, U. (1974). Phys. Lett. 47A, 369.

Shull, C.G. (1968). Phys. Rev. Lett. 21, 1585.

Shull, C.G. (1973). J. Appl. Cryst. 6, 257.

Shull, C.G. and Oberteuffer, J.A. (1972). Phys. Rev. Lett. 29, 871.

Suvorov, E.V. and Polovinkina, V.I. (1974). JETP Lett. 20, 145.

Figures

Fig. 1 - Interference action within one beam of a Three-Crystal-Interferometer.

Fig. 2 - Two-Crystal-Interferometer showing Borrmann fan limitation of radiation within the system.

Fig. 3 - Detail of double Borrmann fan passage of rays in the second crystal plate. Focussing action occurs at the center of the exit face and distributed intensity is found outside the central region.

Fig. 4 - Distribution of intensity released from the exit face in the two directions with scanning of an exit slit across the exit face of the interferometer.

Fig. 5 - Intensity in the central peak with scanning of a 3π-phase step plate across the beam travelling between the two crystal plates.

Fig. 6 - Calculated variation of central peak intensity (BB beam) with 3π-phase step scanning as a function of the magnitude of the interferometer intrinsic phase gradient.

Fig. 7 - Intensity in the central peak with scanning of a 3π-phase step plate with compensation of the interferometer intrinsic phase gradient by an aluminum wedge.

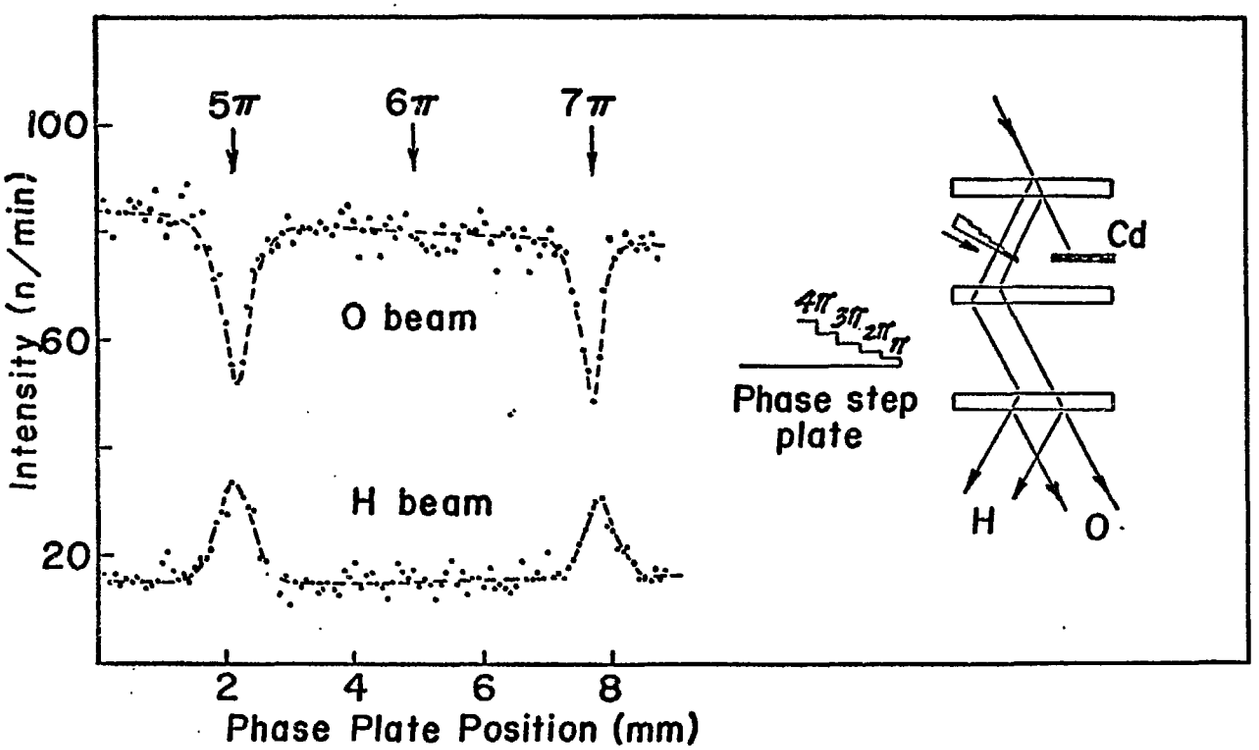

FIG. 1: INTERFERENCE ACTION WITHIN ONE BEAM OF A THREE-CRYSTAL-INTERFEROMETER.

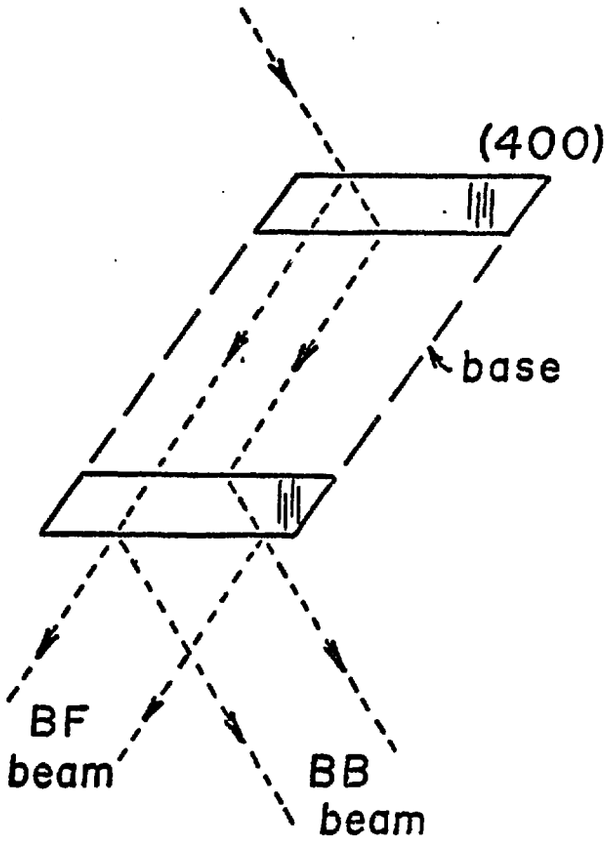

FIG. 2: TWO-CRYSTAL-INTERFEROMETER SHOWING BORRMANN FAN LIMITATION OF RADIATION WITHIN THE SYSTEM.

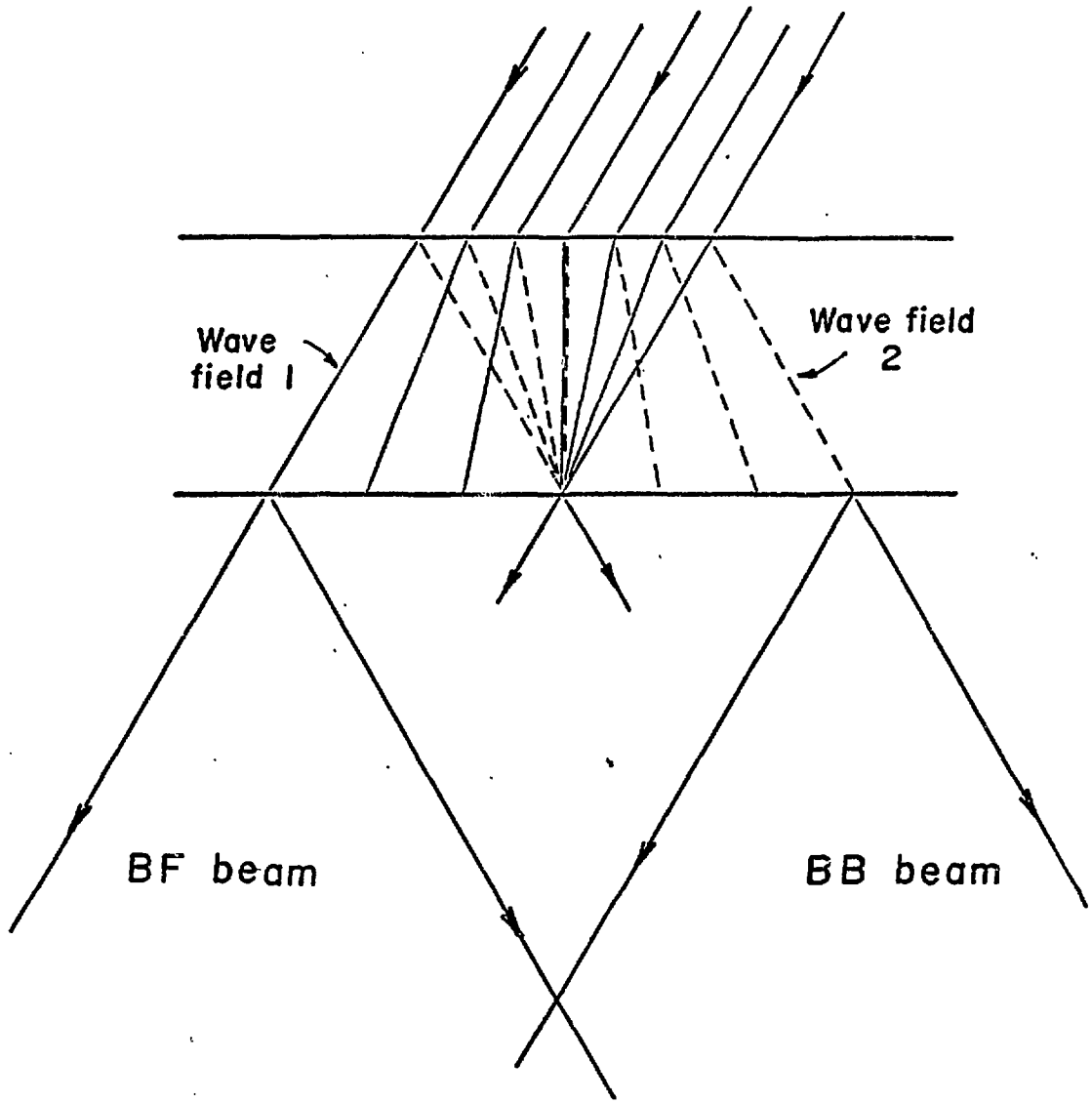

FIG. 3: DETAIL OF DOUBLE BORRMANN FAN PASSAGE OF RAYS IN THE SECOND CRYSTAL PLATE. FOCUSSING ACTION OCCURS AT THE CENTER OF THE EXIT FACE AND DISTRIBUTED INTENSITY IS FOUND OUTSIDE THE CENTRAL REGION.

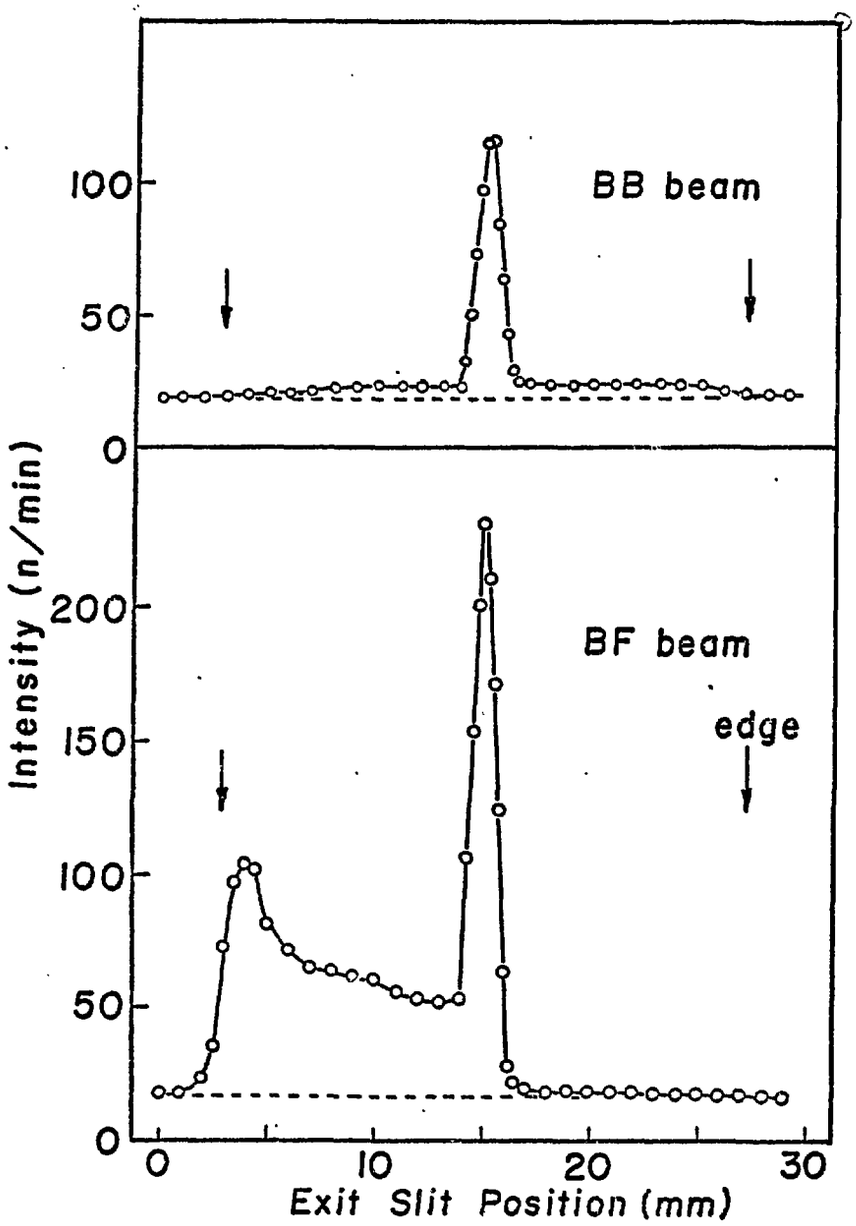

FIG. 4: DISTRIBUTION OF INTENSITY RELEASED FROM THE EXIT FACE IN THE TWO DIRECTIONS WITH SCANNING OF AN EXIT SLIT ACROSS THE EXIT FACE OF THE INTERFEROMETER.

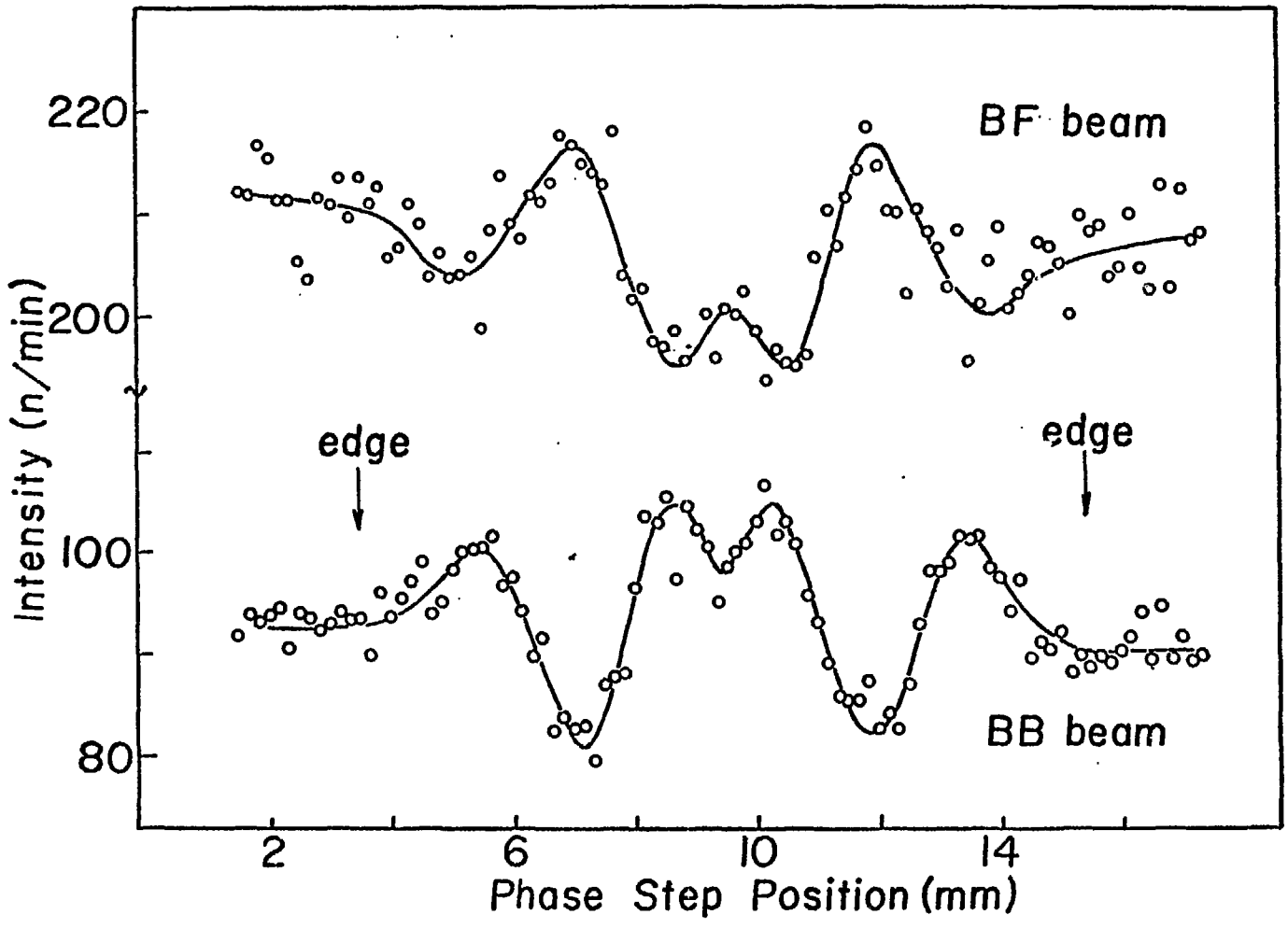

FIG. 5: INTENSITY IN THE CENTRAL PEAK WITH SCANNING OF A 3π-PHASE STEP PLATE ACROSS THE BEAM TRAVELLING BETWEEN THE TWO CRYSTAL PLATES.

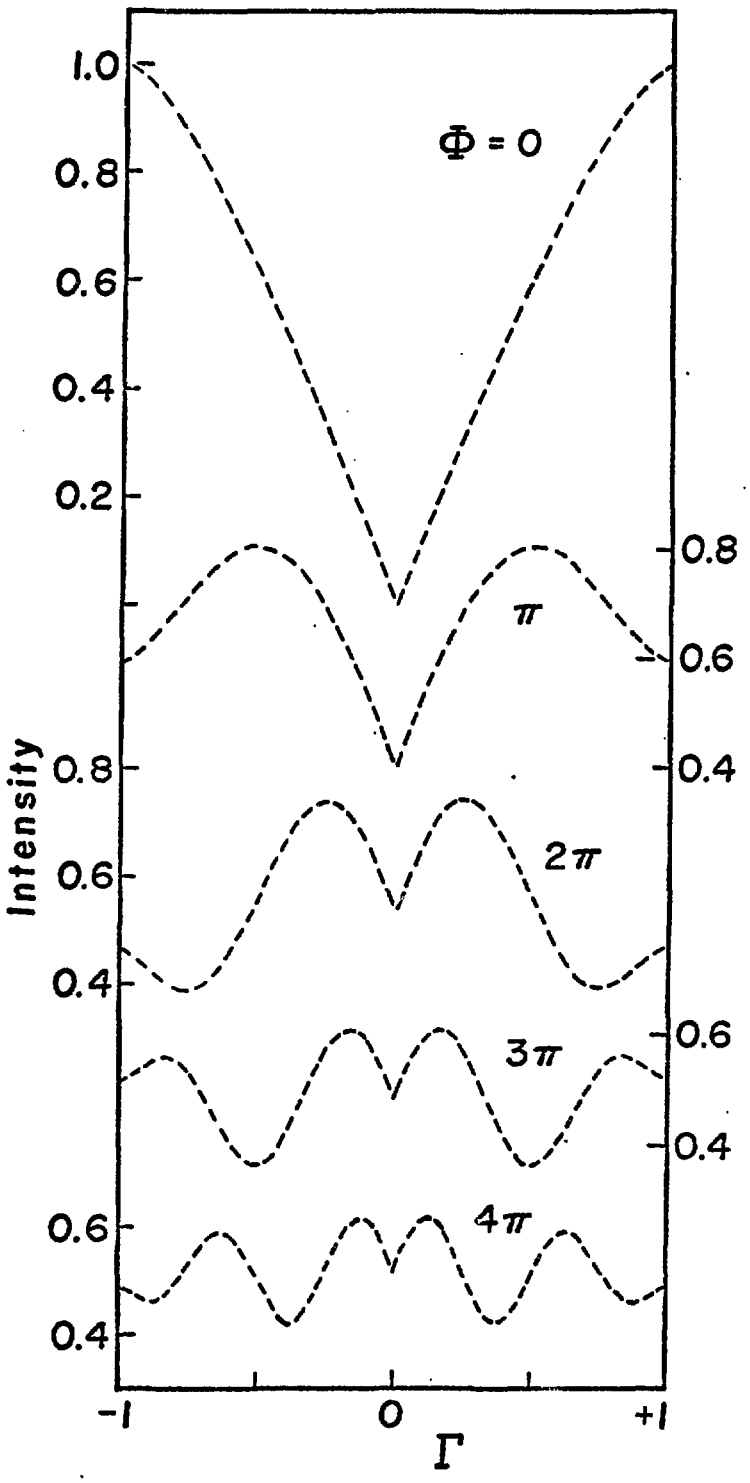

FIG. 6: CALCULATED VARIATION OF CENTRAL PEAK INTENSITY (BB BEAM) WITH 3π-PHASE STEP SCANNING AS A FUNCTION OF THE MAGNITUDE OF THE INTERFEROMETER INTRINSIC PHASE GRADIENT.

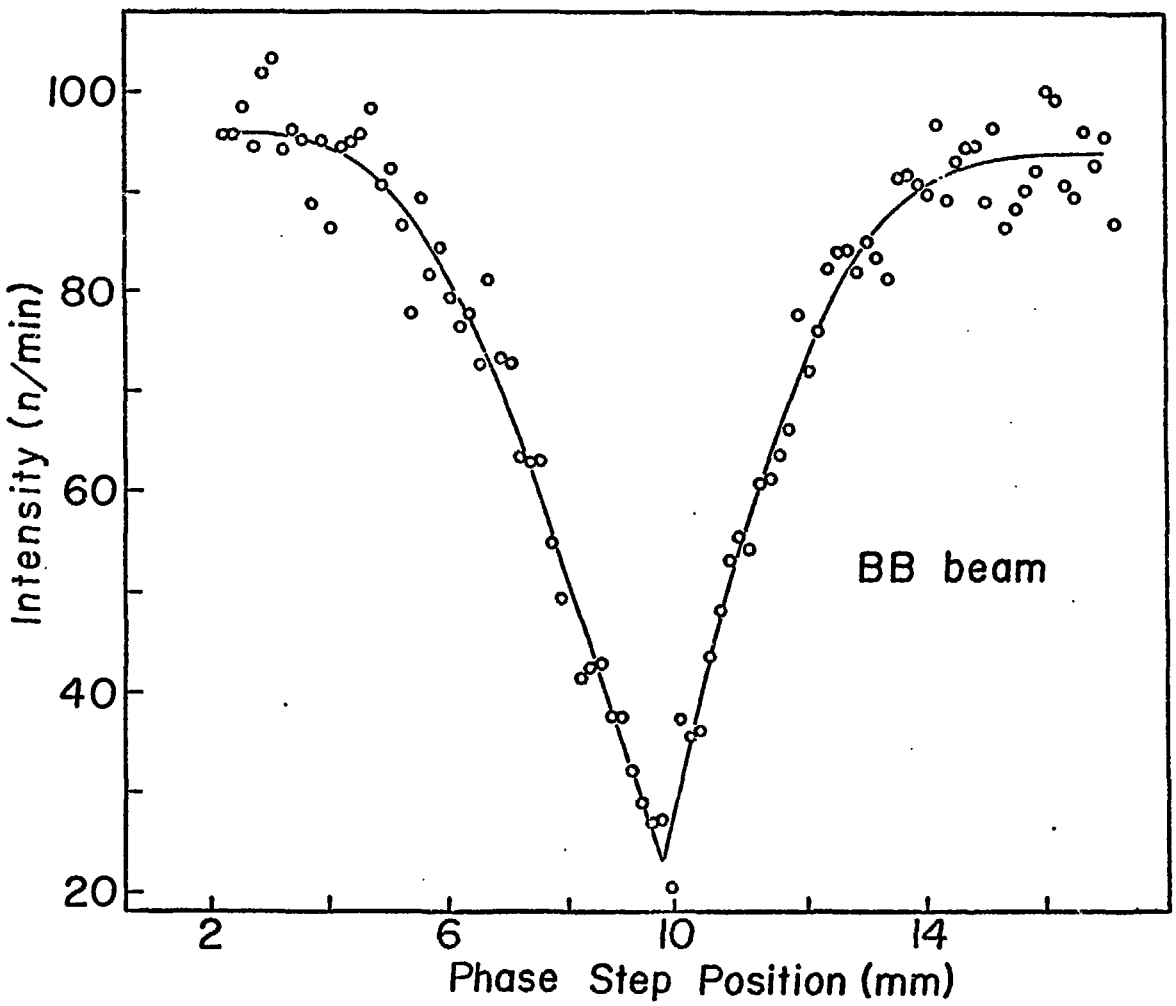

FIG. 7: INTENSITY IN THE CENTRAL PEAK WITH SCANNING OF A 3π-PHASE STEP PLATE WITH COMPENSATION OF THE INTERFEROMETER INTRINSIC PHASE GRADIENT BY AN ALUMINUM WEDGE.